Journal of Applied Mathematics and Computation, 2024, 8(2), 137-143
https://www.hillpublisher.com/journals/JAMC/
ISSN Online: 2576-0653
ISSN Print: 2576-0645

Range and Velocity Walk Correction Algorithm Based on KT-MCICPF

Yongchang Hou[1,2,*], Xuanhe Liu[2], Guanhang Yao[2]

[1]Nanjing Paiyisheng Electronic Technology Co., Ltd., Nanjing, Jiangsu, China.
[2]Nanjing University of Science and Technology, Nanjing, Jiangsu, China.

How to cite this paper: Yongchang Hou, Xuanhe Liu, Guanhang Yao. (2024) Range and Velocity Walk Correction Algorithm Based on KT-MCICPF. *Journal of Applied Mathematics and Computation*, 8(2), 137-143.
DOI: 10.26855/jamc.2024.06.007

Received: May 20, 2024
Accepted: June 18, 2024
Published: July 15, 2024

***Corresponding author:** Yongchang Hou, Nanjing Paiyisheng Electronic Technology Co., Ltd., Nanjing, Jiangsu, China; Nanjing University of Science and Technology, Nanjing, Jiangsu, China.

Abstract

With the development of technology, high-speed targets characterized by high speed, high maneuverability, and strong stealth capabilities pose significant challenges to radar detection performance. In recent years, high-speed target detection has garnered considerable attention in the field of radar signal processing. Increasing the observation time can effectively improve the signal-to-noise ratio of the echoes and the radar's ability to detect weak targets. However, the high speed and maneuverability of the target during an extended observation time can result in range walk and Doppler walk, rendering traditional coherent integration algorithms ineffective. Aiming at a target model moving with uniform acceleration along the radar radial direction, we propose the KT-MCICPF coherent integration algorithm. The proposed algorithm addresses the issues of range walk and Doppler walk, achieving the goals of high-speed target acceleration estimation and coherent integration of target echo signal energy.

Keywords

Long-time coherent integration, Doppler walk, range walk, Keystone transform

1. Introduction

In recent years, with the rapid development of technology and the continuous advancement of stealth technology, the targets for radar detection have become increasingly complex [1-3]. Stealth fighters such as the F-22 and F-35 have emerged [4], along with various cruise missiles, stealth ships, and hypersonic drones. These targets can all be categorized as "long-distance, low-observability, and high-maneuverability" weak targets [5-7]. The common characteristic of these targets is that, whether in the time domain or frequency domain, due to their small radar cross-section and high-speed motion, distant targets are often submerged in strong noise, and the echo energy is limited [8]. As a result, the signal-to-noise ratio of the echo is very low, posing significant challenges to the detection capability and performance of traditional radars. Therefore, improving the detection capability of modern radars for high-speed targets has become a highly focused frontier topic in the radar field [9-12].

This paper addresses the issue of coherent integration gain loss caused by range cell and Doppler walk during long-time coherent integration of high-speed target echoes. The research focuses on the coherent integration algorithm for uniformly accelerated motion and variably accelerated motion models along the radar radial direction. We propose a coherent integration algorithm based on the Keystone Transform and the Modified Coherent Integration Cubic Phase Function (KT-MCICPF). Simulation results indicate that after processing with the MCICPF algorithm, the target echo energy is effectively accumulated in a two-dimensional plane, improving the accuracy of acceleration estimation.

The main steps of this algorithm are as follows:

(1) Perform pulse compression processing on the original radar echo signals.

(2) Determine the target's speed ambiguity number and use the Keystone algorithm to correct the range walk.

(3) Search through the pulse-compressed signals by range cells to identify potential range cells where targets may appear.

(4) Initialize parameters and calculate the instantaneous parameter autocorrelation function of the echo signal in the current range cell.

(5) Perform a non-uniform fast Fourier transform on the delay variable dimension of the instantaneous parameter auto-correlation function, implementing the CPF algorithm. Then, perform a fast Fourier transform on the slow time dimension. This results in a two-dimensional Fourier transform of the autocorrelation function to achieve energy concentration.

(6) Detect peaks based on an appropriate peak detection threshold and record the peak positions.

(7) Estimate the acceleration based on the frequency modulation corresponding to the peak, and construct a compensation function using the estimated acceleration value to compensate for the Doppler walk in the current range cell.

(8) Check whether the compensation for all range cells is complete. If completed, proceed to step 9. If not, return to step 4 to perform compensation for the next range cell.

(9) Perform a Fourier transform (FT) along the slow time dimension for the compensated echo pulse-compressed signals $s_c(t,t_m)$ to complete the coherent integration.

2. Algorithm Derivation

2.1 Echo Model

The echo signal of linear frequency modulation (LFM) radar after downconversion can be expressed as

$$s_{rd}(t,t_m)=A_r\mathrm{rect}\left(\frac{1}{T_P}(t-\frac{2}{c}\sum_{i=0}^{k}\frac{r_i}{i!}t_m^i)\right)\exp(j\pi\mu(t-\frac{2}{c}\sum_{i=0}^{k}\frac{r_i}{i!}t_m^i)^2)\exp(-j\frac{4\pi}{\lambda}\sum_{i=0}^{k}\frac{r_i}{i!}t_m^i) \tag{2.1}$$

When the target is undergoing uniform accelerated motion, i.e., when $k=2$, the echo signal can be simplified as

$$s_{rd}(t,t_m)=A_r\mathrm{rect}(t)\exp(j\pi\mu(t-\frac{2(r_0+v_0t_m+\frac{1}{2}at_m^2)}{c})^2)\exp(-j\frac{4\pi}{\lambda}(r_0+v_0t_m+\frac{1}{2}at_m^2)) \tag{2.2}$$

where A_r represents the amplitude of the attenuated echo signal, τ denotes the delay time, t_m represents slow time, and t represents fast time, r_0 represents the initial distance between the target and the radar, v_0 and a represent the initial velocity and acceleration of the target, respectively.

2.2 Pulse Compression

According to the matched filter theory, this paper performs time-domain pulse compression on the radar echo. The impulse response of the matched filter $h(t)$ is given by

$$h(t)=s_t^*(t_0-t),0<t<t_0 \tag{2.3}$$

Assuming the output of the matched filter is $s_{rm}(t)$, then the output of the matched filter is

$$s_{rm}(t)=s_{rd}(t)*h(t)=\int_{-\infty}^{+\infty}s_{rd}(t-y)h(y)dy \tag{2.4}$$

Performing pulse compression on Equation (2.10) yields

$$s_{rm}(t,t_m)=A_{rm}\mathrm{sinc}\left(B\left(t-\frac{2}{c}\sum_{i=0}^{k}\frac{r_i}{i!}t_m^i\right)\right)\times\exp(-j\frac{4\pi}{\lambda}\sum_{i=0}^{k}\frac{r_i}{i!}t_m^i) \tag{2.5}$$

Here, A_{rm} is the amplitude of the signal after pulse compression, and $\mathrm{sinc}(x)=\sin x/x$ is known as the sinc function.

From Equation (2.14), it can be seen that pulse compression can improve the signal-to-noise ratio (SNR) of the target echo. After pulse compression processing, the output SNR is improved. However, higher-order motion parameters of the target can cause mismatches in the matched filter, resulting in peak point shifts.

2.3 Keystone Transform

Based on the radar echo model established above, the echo of a single uniformly accelerated target after pulse compression can be expressed as

$$s_p(t,t_m') = A\sin c(t-\frac{2R(t_m')}{c})\exp(-j2\pi f_c\frac{2R(t_m')}{c}) \tag{2.6}$$

Applying the Keystone transform to equation (2.6) yields

$$S_p(f,t_m)=A_c\mathrm{rect}(\frac{f}{B})\exp(-j\frac{4\pi f}{c}R_0+j\frac{2\pi f}{c}at_m{}^2-j\frac{4\pi}{\lambda}R_0-j\frac{4\pi}{\lambda}v_0t_m-j\frac{2\pi}{\lambda}at_m{}^2) \tag{2.7}$$

Where, for a generally uniformly accelerating moving target, the range offset caused by the acceleration of the moving target that is not corrected by the first-order Keystone transform can be ignored. Under this premise, ignoring the range offset caused by the target acceleration in equation (2.7) and transforming it to the time domain plane yields

$$s_p(t,t_m) = A\sin c(t-\frac{2R_0}{c})\exp[-j\frac{4\pi}{\lambda}(R_0+v_0t_m+\frac{1}{2}at_m{}^2)] \tag{2.8}$$

2.4 Principles of the MCICPF Algorithm

The pulse-compressed signal after the Keystone transform has its energy accumulated in the same range cell. By extracting and analyzing the signal along the slow-time dimension, it can be observed that the echo signal in the range cell where the target is located can be modeled 0as an LFM signal along the slow-time dimension. Assuming that after the Keystone transform, the range walk is corrected and the target range is R_0 , the slow-time signal of the radar echo in the range cell where the pulse-compressed peak is located can be expressed as

$$s_p(\frac{2R_0}{c},t_m) = A\exp[-j\frac{4\pi}{\lambda}(R_0+v_0t_m+\frac{1}{2}at_m{}^2)] \tag{2.9}$$

The CPF algorithm essentially achieves parameter estimation of LFM signals through the Non-Uniform Fast Fourier Transform (NUFFT). CPF is defined as

$$\mathrm{CPF}\left(t_m,f_{\tau^2}\right)=\int R_{\mathrm{CPF}}(t_m,\tau)\exp\left(-j2\pi f_{\tau^2}\tau^2\right)d\tau^2 \tag{2.10}$$

where, τ is the delay time variable, f_{τ^2} is the corresponding frequency variable of τ^2, and $R_{\mathrm{CPF}}(t_m,\tau)$ is the transformation kernel of the CPF algorithm, defined as

$$R_{\mathrm{CPF}}(t_m,\tau)=s_p(t_m+\tau)s_p(t_m-\tau) \tag{2.11}$$

Substituting equation (2.9) into equation (2.11) yields

$$R_{\mathrm{CPF}}(t_m,\tau)=|A|^2\exp\left[-j\frac{8\pi}{\lambda}\left(R_0+v_0t_m+\frac{1}{2}at_m^2+\frac{1}{2}a\tau^2\right)\right] \tag{2.12}$$

Substituting equation (2.12) into equation (2.10) yields

$$\mathrm{CPF}\left(t_m,f_{\tau^2}\right)=A^2\exp\left[-j\frac{8\pi}{\lambda}\left(R_0+v_0t_m+\frac{1}{2}at_m^2\right)\right]\delta\left(f_{\tau^2}+\frac{2a}{\lambda}\right) \tag{2.13}$$

where, f_{τ^2} is the frequency component with respect to the delay variable τ .

In equation (2.14), it can be seen that $\mathrm{CPF}\left(t_m,f_{\tau^2}\right)$ peaks at $f_{\tau^2}=-2a/\lambda$. In the 2D plane of $t_m-f_{\tau^2}$, the energy of the processed echo signal is linearly distributed along $f_{\tau^2}=-2a/\lambda$ parallel to the slow time axis. From this observation, although the estimation of the quadratic phase coefficient can be obtained, the signal-to-noise ratio and resolution are relatively low at this point, leading to some errors in parameter estimation. Additionally, during multi-target detection, cross-term and spurious peak interference are inevitably produced. The presence of t_m^2 in the echo signal causes the peak to be less concentrated, so direct integration along t_m is not feasible. CPF does not have the capability to suppress cross-terms and spurious peaks.

We propose an improved CPF coherent accumulation algorithm on the basis of CPF. Then we can yield

$$\mathrm{MCICPF}\left(f_d, f_{\tau^2}\right) = A^2 \exp\left(-j\frac{8\pi}{\lambda}R_0\right)\delta\left(f_d + \frac{4v_0}{\lambda}\right)\delta\left(f_{\tau^2} + \frac{2a}{\lambda}\right) \tag{2.14}$$

The compensated echo can be expressed as

$$s_c(t,t_m) = A\sin c(t - \frac{2R_0}{c})\exp[-j\frac{4\pi}{\lambda}(R_0 + v_0 t_m + \frac{1}{2}(a - \hat{a})t_m{}^2)] \tag{2.15}$$

When $\hat{a} = a$, the Doppler shift can be completely compensated.

3. Algorithm Simulation

To verify the effectiveness of the proposed algorithm, a simulation of the target detection process is conducted. The radar simulation parameters are shown in Table 1. The KT-MCICPF algorithm estimates the target's second-order phase coefficient and compensates for the Doppler shift caused by the second-order phase coefficient. The following simulation demonstrates the coherent integration process of a single uniformly accelerating target in a noise-free environment based on the KT-MCICPF algorithm.

Table 1. Radar parameters for KT-MCICPF algorithm simulation

Simulation Parameters	Simulation value	Simulation Parameters	Simulation value
Carrier Frequency	4GHz	Sampling frequency	80MHz
Pulse width	8us	Pulse interval time	200us
Transmit signal bandwidth	40MHz	Number of accumulation cycles	512

3.1 Range Walk Correction

Set the target's initial position $R_0 = 3000$ m, velocity $v_0 = 480$ m/s, and acceleration $a = 200$ m/s^2. Figure 1(a) shows the pulse compression result of the echo before range walk correction, and Figure 1(b) shows the coherent integration result before range walk correction. It is evident that due to the target's high speed and acceleration, there are phenomena of range walk and Doppler walk in the echo signal. Figure 1(c) presents the pulse compression result of the echo after range walk correction using the Keystone transform. It can be seen that the Keystone transform corrects the range walk of the target echo. Figure 1(d) displays the coherent integration result after range walk correction using the Keystone transform. The results indicate that the Keystone transform provides effective correction for the range walk of radar echoes from uniformly accelerating targets. However, the energy after integration is still distributed across multiple Doppler cells, with a velocity offset of 20 m/s, indicating that the Doppler walk still exists, as shown in Figure 1(e).

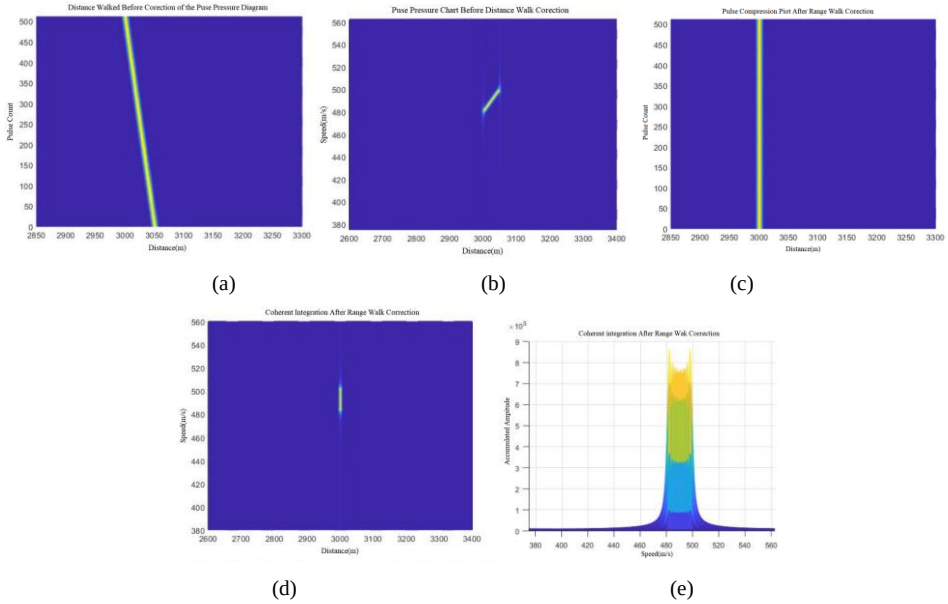

Figure 1. Results of Keystone Transform for Range Walk Correction of Uniformly Accelerating Target: (a) Before correction (b) Coherent integration before correction (c) After correction (d) Coherent integration after correction (e) Doppler domain coherent integration result.

3.2 Doppler Walk Correction

Figure 2(a) shows the result of computing the instantaneous parameter autocorrelation of the current range cell echo signal. By introducing a new time delay variable to translate the original signal, the one-dimensional echo signal is transformed into a two-dimensional plane. This transformation facilitates subsequent energy accumulation of the echo signal, thereby improving the accuracy of parameter estimation.

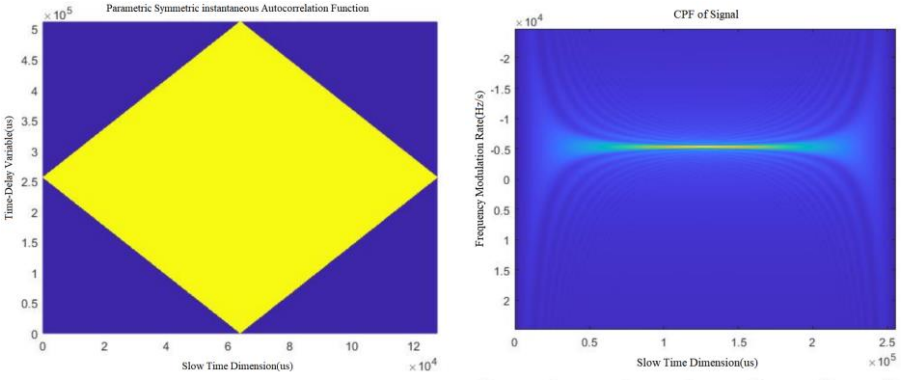

(a) (b)

Figure 2. Symmetric Instantaneous Autocorrelation Function of the Parameters.

Figure 2(b) shows the results after processing with the CPF algorithm. As can be seen from the figure, the CPF algorithm eliminates the influence of the time delay variable. On the two-dimensional plane of the slow time variable and the modulation frequency, the energy of the echo signal processed by the CPF algorithm is distributed linearly along the $f_{\tau^2} = -2a/\lambda$, parallel to the slow time axis. However, at this time, the signal-to-noise ratio (SNR) of the echo signal is relatively low, and the energy is dispersed along a straight line, making it susceptible to noise interference. Additionally, the current resolution is insufficient. To ensure the reliability and accuracy of the target acceleration estimation, the MCICPF algorithm needs to be used. By accumulating energy in both dimensions to form a peak, the SNR is improved, ensuring the accuracy of parameter estimation.

Figure 3(a) shows the results of the signal processed by the MCICPF algorithm. From the figure, it can be seen that through the joint accumulation in two dimensions, a peak containing the target acceleration information has been formed in the two-dimensional plane $f_d - f_{\tau^2}$. According to Figure 3(b), the frequency modulation rate corresponding to the peak can be used to derive the estimated acceleration value and compensate for the target acceleration. Based on the information in the figure, the frequency modulation rate is Hz/s, and the estimated acceleration value is 199.99 m/s².

Based on the obtained estimated acceleration value, a compensation function is constructed to perform acceleration compensation. After compensating for the acceleration, coherent integration is applied to the target echo, resulting in the outcome shown in Figure 3(c). From the figure, it is evident that in the range cell where the target is located, the coherent integration after acceleration compensation shows a significant improvement in accumulation gain. Furthermore, from the Doppler distribution diagram of the coherently integrated signal after acceleration compensation shown in Figure 3(d), it can be seen that the Doppler shift of the compensated echo signal disappears.

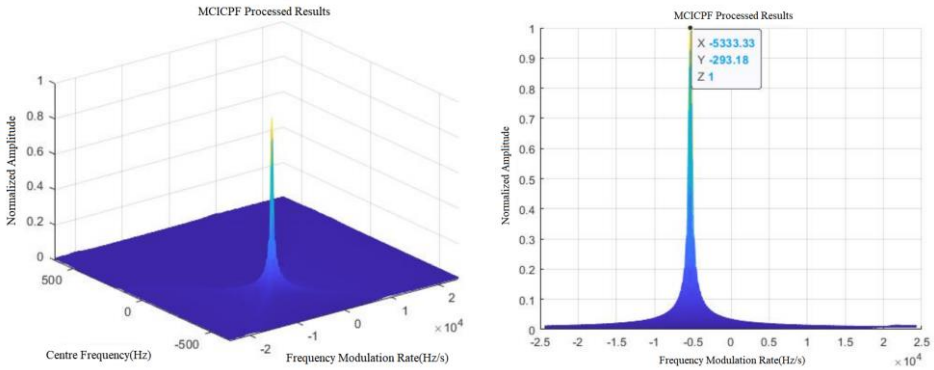

(a) (b)

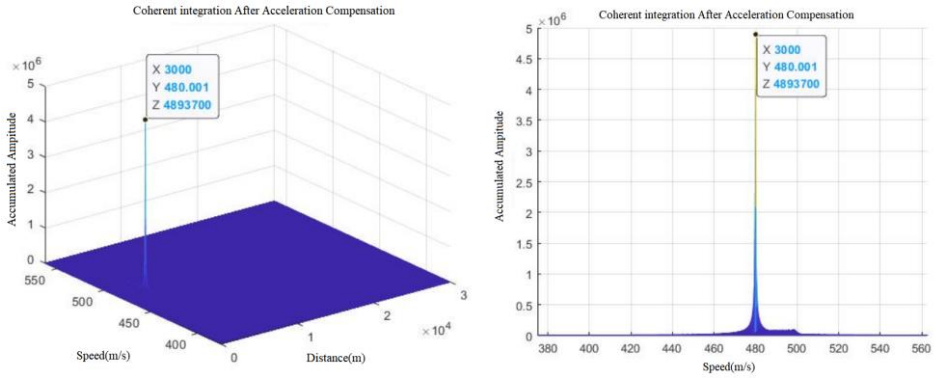

(c) (d)

Figure 3. (a) MCICPF Algorithm Processing Result (b) Frequency Modulation Result after MCICPF Algorithm Processing (c) Coherent Integration after Acceleration Compensation (d) Distribution of Coherent Integration after Acceleration Compensation along Doppler Dimension.

4. Algorithm Complexity Analysis

The KT-MCICPF algorithm mainly involves two core algorithms, the Keystone transform and the MCICPF algorithm. Let the number of range cells and the number of accumulated pulses be denoted as N and M respectively. The Keystone transform implemented using the sinc interpolation method has a complexity of $O[NM^2 + MN(M-1)]$, then performs MCICPF processing, The complexity of the MCICPF process, which can be implemented using only one Non-uniform Fast Fourier Transform (NUFFT) and one FFT, is therefore $O[2M^2 \log_2 M]$. Consequently, the computational complexity of the KT-MCICPF algorithm can be expressed as $O[2M^2 \log_2 M + NM^2 + MN(M-1)]$.

5. Conclusion

This paper proposes an algorithm based on KT-MCICPF for a target model undergoing uniformly accelerated motion along the radar radial direction. The Doppler walk problem in radar echo processing is addressed using a cubic phase function based on improved coherent accumulation. The proposed algorithm does not require parameter searching, interpolation operations, or nonlinear transformations from Cartesian to polar coordinates. It can be efficiently implemented using only NUFFT and FFT, significantly reducing computational complexity and enhancing real-time performance.

References

[1] C. L. Luengo. Hendriks, M. van. Ginkel, PW. Verbeek, et al. The generalized radon transform: Sampling, accuracy and memory considerations [J]. Pattern Recognition, 2005, 38(12): 2494-2505.

[2] G. Koukiou, V. Anastassopoulos. 3-D FFT moving object signatures for velocity filtering [J]. Aceee International Journal of Signal and Image Processing, 2014, 5(1): 71-75.

[3] Y. He, T. Jian, F. Su, et al. A method for MTD detectability improvement using FFT/WFFT-DWT [C]. CIE International Conference on Radar., 2006:1480-1483.

[4] X, Jia, Y. Ji, Y. N. Peng, et al. Radon-fourier transform for radar target detection, I: generalized doppler filter bank [J]. IEEE Transactions on Aerospace and Electronic Systems, 2011, 47(2):1186-1202.

[5] B. Min, B. Y. Jia, L. Guo, et al. Coherent integration for maneuvering target detection at low SNR based on radon-general linear chirplet transform [J]. IEEE Geoscience and Remote Sensing Letters, 2022, 19:1-6.

[6] Z. J. Li, Q. L. Zhang, L. Yu, et al. Long-time coherent integration of the maneuvering weak target for wideband radar based on ACCF-LVD-KT. EEI 2022; 4th International Conference on Electronic Engineering and Informatics, Guiyang, China, 2022: 1-5.

[7] X. L. Chen, J. Guan, J. B. Zheng. Radar fast long-time coherent integration via TR-SKT and robust sparse FRFT [J]. System Engineering and Electronics, 2023, 34(5):1116-1129.

[8] Y. X. Zhang, H. W. Xu. A wideband/narrowband fusion-based motion estimation method for maneuvering target [J]. IEEE Sensors Journal, 2019, 19(18): 8095-8106.

[9] J. Zheng, H. Liu, J. Liu, et al. Radar high-speed maneuvering target detection based on three-dimensional scaled transform [J]. IEEE Journal of Selected Topics in Applied Earth Observations and Remote Sensing, 2018, 11(08): 2821-2833.

[10] Y. Yang, M. Fang, C. Zhao, et al. An efficient coherent integration method for high-speed maneuvering target with nonlinear motion. 2021 CIE International Conference on Radar (Radar), Haikou, Hainan, China, 2021: 2350-2355.

[11] X. Li, G. Cui, W. Yi, et al. Coherent integration for maneuvering target detection based on radon-Lv's distribution [J]. IEEE Signal Processing Letters, 2015, 22(9):1467-1471.

[12] J. B. Huang, R. Tao. Fractional fourier transform and its application to SAR imaging of moving targets [C]. Proceedings of 2009 2nd Asian-Pacific Conference on Synthetic Aperture Radar (APSAR2009). China Institute of Electronics (CIE), 2009: 743-746.